Decontamination of Methylene Blue from Aqueous Solution by Rhamnolipid-modified Biochar

Meinan Zhen, Jingchun Tang,* Benru Song, and Xiaomei Liu

To remove methylene blue (MB) from water, rhamnolipid-modified biochar (BC-RL) was synthesized *via* a facile method. The surface structures and properties of the biochar (BC) and BC-RL were characterized by scanning electron microscopy, Fourier transform infrared spectra, X-ray diffraction spectra, X-ray photoelectron spectra, N_2 adsorption-desorption isotherms, and Raman spectra. The results showed that modification with rhamnolipid remarkably increased the functional groups on the BC-RL, but reduced the surface area. The MB removal efficiency of the BC-RL increased with an increase in the adsorbent loading and temperature. Moreover, the adsorption performance of the BC-RL was obviously higher than that of the BC, which was mainly attributed to the increased number of functional groups. The adsorption kinetic data was fitted well to the pseudo-second-order model with a coefficient of determination greater than 0.999. The coefficients of determination of the adsorption isotherm fitted by different models decreased in the following order: BET > Freundlich > Langmuir. This indicated that the adsorption of MB onto the BC-RL involves a multilayer formation process. These results suggested that the BC-RL could be an environmentally benign and cost-effective adsorbent for the removal of MB from aqueous solutions.

Keywords: Adsorption; Rhamnolipid; Biochar; Methylene blue; Kinetic; Isotherm

Contact information: Key Laboratory of Pollution Processes and Environmental Criteria (Ministry of Education), Tianjin Engineering Research Center of Environmental Diagnosis and Contamination Remediation, College of Environmental Science and Engineering, Nankai University, Tianjin 300071, China;
** Corresponding author: tangjch@nankai.edu.cn;*

INTRODUCTION

In recent years, substantial amounts of wastewater have been produced in the textile, leather, paper, plastics, metallurgy, and other industries (Wu *et al*. 2014). These industries have produced over 7×10^5 tons of dyestuffs each year (Negueroles *et al.* 2017). It has been reported that methylene blue (MB), one of the most widely used dyes, can induce permanent injury, such as eye burns, in both humans and animals (Han *et al.* 2015; Kermanioryani *et al.* 2016). The release of dyes, especially MB, into the environment have resulted in serious environmental pollution all over the world, which poses a potential risk to human beings and ecosystems (Wu *et al.* 2014; Kermanioryani *et al.* 2016). Therefore, it is of great importance to develop cost-effective and environmentally friendly technologies to remove dyes from effluents before discharging them into the natural environment. Various approaches, including advanced chemical oxidation, photo-degradation, membrane treatment, biological treatment, and adsorption treatment, have been studied to remove MB from industrial wastewater to alleviate the associated environmental problems (Chen *et al.* 2017; Negueroles *et al.* 2017; Ribeiro *et al.* 2017).

Among these methods, the adsorption treatment has attracted much attention because of its relatively low cost, easy operation, lower sensitivity to toxic pollutants, and high efficiency (Mohan *et al.* 2014).

Carbon-based materials have been widely applied for removing organic and inorganic pollutants from water and remediating contaminated soil because of their high surface areas and abundant functionality (Beesley *et al.* 2011; Zheng *et al.* 2013; Inyang and Dickenson 2015; Tan *et al.* 2015). Currently, activated carbon (AC) is one of the most widely used environmental remediation materials because of its porous internal structure and large specific surface area. Recently, carbon nanotubes, graphene, and graphene oxide, as well as their derivatives and composite materials, have been greatly developed and studied for numerous environmental applications (Xu *et al.* 2012; Hou *et al.* 2016; Wang *et al.* 2016b; Ersan *et al.* 2017; Kumar *et al.* 2017). As a result of their specific structures and large surface areas, they have exhibited better performances at removing organic and inorganic pollutants from water than conventional AC (Xu *et al.* 2012; Gaber *et al.* 2017). However, the large-scale employment of these materials seems impracticable considering their high cost and complicated and energy-consuming synthesis process, as well as the potential risks they pose to human health and ecosystems (Hu and Zhou 2013). In contrast, biochar (BC)-based materials, which are produced from renewable lignocellulosic biomass, are suitable for practical application because they are abundant, cheap, and environmentally friendly compared with other carbon-based materials (Ashworth *et al.* 2014; Liu *et al.* 2015; Hou *et al.* 2017). The production of BC from biomass through pyrolysis is both cost-effective and environmentally sustainable because of the renewability, natural abundancy and low cost of biomass, reduction of greenhouse gas emissions, and production of large amounts of by-products, including bio-oil and gas (Hou *et al.* 2015; Liu *et al.* 2015; Ma *et al.* 2017; Hou *et al.* 2018). Nevertheless, BC-based materials have generally exhibited lower adsorption capacities than conventional AC because of their relatively small specific surface areas (Deng *et al.* 2014; Liu *et al.* 2016).

The structure and properties of BC can be regulated by an elaborate selection of the proper biomass precursor, pyrolysis conditions, catalyst, and post-modification treatment, and thus their decontamination performance can be greatly enhanced (Liu *et al.* 2015, 2016). Because the adsorption performance of BC is mainly controlled by its surface area, porous structure, and surface chemistry, it is of great importance to develop innovative strategies to engineer BCs with good porous structures and surface chemistries (Ma *et al.* 2017). Although many carbon-based nanomaterials with unique structures and properties have been developed, an effective design and control of the porous structure for waste-derived BC has still not been achieved in a cost-effective and environmentally friendly way (Xi *et al.* 2014; Ding *et al.* 2017). The employment of large amounts of chemical activation agents, a high activation temperature, and a long activation time have led to high costs for the final products and associated environmental concerns. Additionally, several recent investigations have indicated that a large specific surface area might not result in a constant increase in the adsorption capacity of organics because micropores (< 2 nm) may suppress the diffusion of foreign interacting species (Suhas *et al.* 2016).

Another way to tailor the properties of BCs is by introducing functional groups to the surface through post-treatment. For instance, Chen *et al.* (2015) and Cui *et al*. (2017) reported that treating cotton-derived carbon materials with HNO_3 could increase the oxygen-containing functional groups content without altering their porous structure and specific surface area, leading to a remarkable improvement in the adsorption efficiency of organic pollutants. Recently, surfactants, which are capable of regulating the interface

characteristics between aqueous and non-aqueous liquids, have been found to be effective for improving the adsorption efficiency of carbon-based materials (Wu *et al.* 2013, 2014). For instance, cetyltrimethylammonium bromide-modified graphene demonstrated an improved Cr(VI) removal efficiency from aqueous solutions because of the introduction of oxygen-containing groups onto the surface of the graphene (Wu *et al.* 2013). Therefore, the modification of BC with bio-surfactants may provide a low-cost, effective, and environmentally friendly way to improve the adsorption efficiency of BCs.

In this work, rhamnolipid, an environmentally friendly bio-surfactant produced by microorganisms, was used to modify a BC to enhance the adsorptive removal of MB from water. To investigate the surface structures and properties of the BC and rhamnolipid-modified BC (BC-RL), the synthesized materials were characterized with scanning electron microscopy (SEM), Fourier transform infrared (FTIR) spectra, X-ray diffraction (XRD) spectra, X-ray photoelectron (XPS) spectra, and N_2 adsorption-desorption isotherms. The influence of the adsorbent loading, MB concentration, composition, and structure of the adsorbent on the adsorption of MB were investigated. Moreover, the adsorption kinetics and isotherms were analyzed to elucidate the adsorption mechanism.

EXPERIMENTAL

Materials

Rice husk was collected locally in Tianjin, China, repeatedly washed with deionized (DI) water to remove dirt, and then dried in an oven at 60 °C. Rhamnolipid (> 90%) was purchased from Dingguo Biological Technology Co. Ltd (Tianjin, China). Methylene blue trihydrate ($C_{16}H_{18}ClN_3S \cdot 3H_2O$, 99% in purity, pKa = 2.6) was obtained from Tianjin Heowns Biochem LLC (Tianjin, China). All of the other chemical reagents were purchased from commercial sources in China and were used as received.

Preparation of the Biochar

The dried rice husk was loosely placed in a muffle furnace and treated at the desired temperatures (300 °C, 500 °C, and 700 °C) under oxygen-limited conditions for 3 h. The BC was ground to pass through a 0.50-mm sieve. After pyrolysis, the samples were washed with DI water several times to remove impurities, oven-dried at 80 °C, and stored in a desiccator before use. The BCs prepared at 300 °C, 500 °C, and 700 °C were named 300BC, 500BC, and 700BC, respectively.

Synthesis of the Rhamnolipid-modified Biochar

The BC-RL was synthesized according to the method previously reported by Wu *et al.* (2013). Briefly, 1 g of BC (300BC, 500BC, and 700BC) was dispersed into 100 mL of DI water and sonicated for 1 h. Six hundred milligrams of rhamnolipid was dissolved in 100 mL of DI water and added to the BC suspension. The obtained suspension was stirred with sonication at room temperature for 24 h. Subsequently, the black solid precipitate was separated through centrifugation, and washed with anhydrous ethanol and DI water five times each. Finally, the BC-RL samples, which were labelled 300BC-RL, 500BC-RL, and 700BC-RL, were dried at 80 °C for 24 h.

Characterization of the Biochar and Rhamnolipid-modified Biochar

The microscopic features and morphologies of the BCs and BC-RLs were observed using a JSM-7800 field emission scanning electron microscope (JEOL, Tokyo, Japan). The Brunauer-Emmett-Teller (BET) specific surface area and pore distribution of the samples were measured with N_2 adsorption-desorption isotherms using a Chemisorption Analyzer (ChemiSorb 2720, Micromeritics, Georgia, USA). To investigate the crystal structure of the samples, the XRD patterns were recorded with an Ulitma IV diffractometer (Rigaku, Tokyo, Japan) using Cu Kα radiation and a scanning rate of 5°/min. The Raman spectra were recorded on a RTS-HiR-AM Raman spectrometer (TEO, Beijing, China) with a laser frequency of 514 nm as an excitation source. The surface functional groups were investigated using XPS and FTIR spectroscopy. The XPS data was collected on an ESCALAB 250Xi X-ray photoelectron spectrometer (Thermo Scientific, Miami, USA) with a monochromatic Al Kα X-ray excitation source. The samples were dried and then evacuated into the analysis chamber to high vacuum (lower than 10−6 Pa) prior to the measurement. The measurement was conducted at a power of 300 W by transient energy of 160 eV with a step size of 1 eV. The binding energy scale was calibrated using standard samples: Au $4f_{7/2}$ (83.95.0eV), Ag $3d_{5/2}$ (368.2eV) and Cu $2p_{3/2}$ (932.6eV). The FTIR spectra were recorded on a TENSOR 37 IR spectrometer (BRUKER, Karlsruhe, German) with a resolution of 4 cm^{-1} in the transmission mode. The KBr-disk method was used to prepare the test samples.

Adsorption Experiments

The batch adsorption experiments were conducted in 50-mL polyethylene test tubes. The concentration of the 25-mL MB solution varied from 50 mg/L to 200 mg/L, and the pH was adjusted to 7.0. A certain amount of BC or BC-RL (10 mg to 100 mg) was added to the MB solution as the adsorbent. After gentle shaking for the desired time (5 min, 10 min, 15 min, 30 min, 1 h, 2 h, 4 h, 6 h, 9 h, 12 h, 16 h,18 h, and 24 h), all the suspension in the tube was subjected to solid-liquid separation using 0.2-μm syringe filters immediately, and the supernatant was obtained. The concentration of the MB was measured at 665 nm (the maximum absorption wavelength of MB) using an ultraviolet visible spectrophotometer (T6, PERSEE, Beijing, China). The adsorbed quantity and removal efficiency of the MB was calculated according to Eqs. 1 and 2, respectively,

$$q_e = \frac{(C_0 - C_e) \times V}{m} \quad (1)$$

$$r_e = \frac{C_0 - C_e}{C_0} \times 100\% \quad (2)$$

where q_e corresponds to the adsorbed quantity (mg/g), r_e is the removal efficiency (%), C_0 and C_e represent the initial and equilibrium concentrations of the MB (mg/L), respectively, V is the volume of the suspension (mL), and m is the weight of the adsorbent (g). The experiments were conducted in triplicate. Relative errors of the data were less than 3%.

RESULTS AND DISCUSSION

Structures and Properties of the BCs and BC-RLs

Morphology and structure

The morphologies of the BCs and BC-RLs were observed with SEM images. Figure 1 shows that the 300BC retained some original cell structures because of insufficient degradation of the biomass. As the pyrolysis temperature increased, the original cell structures were disrupted gradually, the bulk structure was transformed into particles with much smaller sizes, and the porosity of the BCs increased. These phenomena were in accordance with previous reports (Zhang *et al.* 2015). Moreover, it was observed that the morphologies of the BC-RLs were similar to that of the corresponding BCs prepared at the same temperature, which suggested that modification with rhamnolipid had little impact on the morphology.

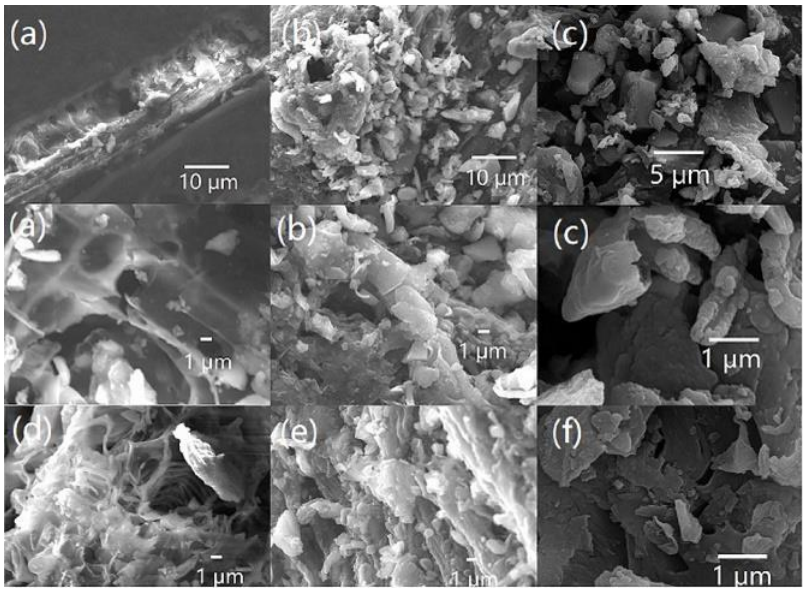

Fig. 1. SEM images of the 300BC (a), 500BC (b) and 700BC (c), 300BC-RL (d), 500BC-RL (e) and 700BC-RL (f)

The N_2 adsorption-desorption isotherms and pore size distribution curves of the BCs and BC-RLs are shown in Fig. 2. The specific surface area (S_{BET}), pore volume (V_{pore}), and average pore diameter ($D_{average}$) are listed in Table 1. The S_{BET} and V_{pore} of the BCs and BC-RLs increased with an increase in the pyrolysis temperature. However, the S_{BET} and V_{pore} of the BC-RLs were remarkably lower than those of the corresponding BCs. Previous study also showed that the S_{BET} of graphene oxide reduced remarkably after modification by Rhamnolipid (Wu *et al*. 2014). The $D_{average}$ values of the BC-RLs were larger than those of the corresponding BCs. On one hand, some rhamnolipid may bond on the internal surface of BCs, thus blocking some small pores in the BCs. On the other hand, some BCs particle may agglomerate owing the binding effect of rhamnolipid. As a consequence, the S_{BET} and V_{pore} of the BC-RLs were lower than those of the corresponding BCs.

Table 1. Textural Properties of the Synthesized BCs and BC-RLs

	300BC	300BC-RL	500BC	500BC-RL	700BC	700BC-RL
S_{BET} (m^2/g)	2.8	2.5	226.7	58.8	285.5	75.4
V_{pore} (cm^3/g)	0.011	0.010	0.108	0.020	0.115	0.053
$D_{average}$ (nm)	15.2	16.5	1.9	4.6	1.9	2.6

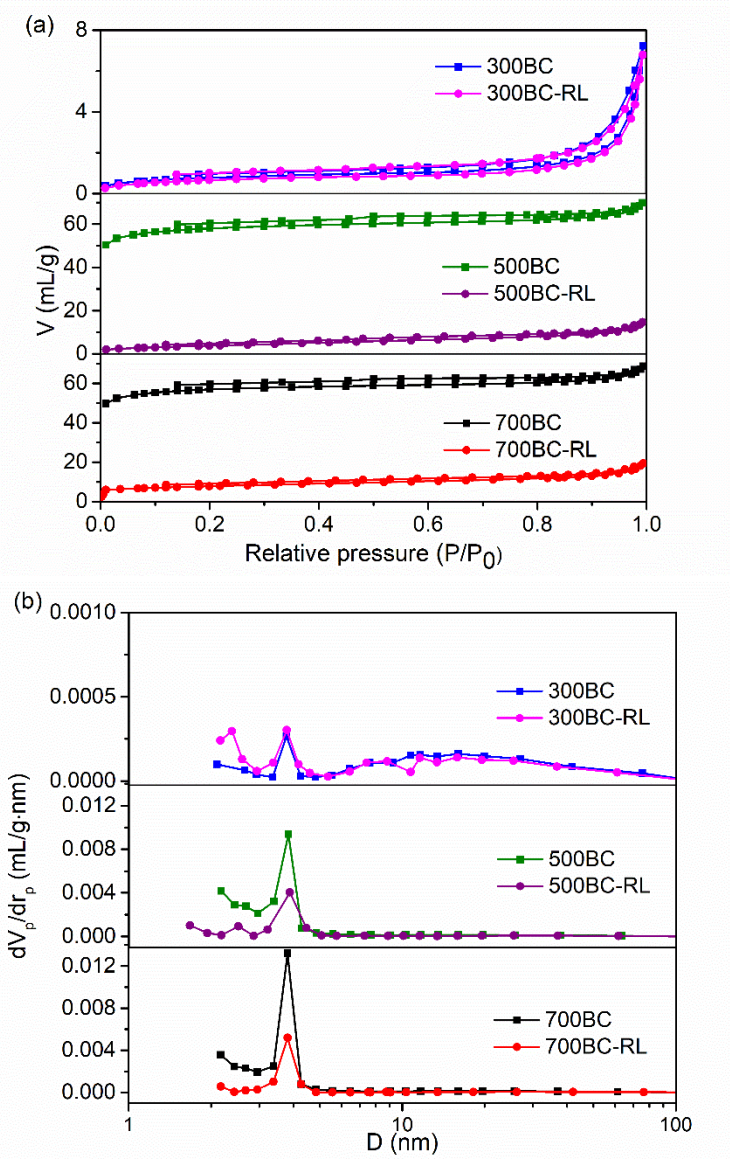

Fig. 2. (a) N_2 adsorption-desorption isotherms and (b) pore size distribution curves of the BCs and BC-RLs

Functional groups

The functional groups of the BCs and BC-RLs were analyzed using FTIR and XPS spectra. Several characteristic peaks (Fig. 3), including O-H (3440 cm^{-1}) and Si-O symmetrical stretching vibration (798 cm^{-1} and 466 cm^{-1}), were observed in the FTIR

spectra of the 300BC and 500BC (Zheng *et al.* 2013; Hou *et al.* 2015). These peaks, except for the O-H peak (3440 cm^{-1}), were also observed in the FTIR spectra of the 700BC. In contrast, there were several new peaks in the BC-RLs, including at 2982 cm^{-1}, 2902 cm^{-1}, 1633 cm^{-1}, and 1385 cm^{-1} that were attributed to the asymmetric stretching vibration of CH_3, asymmetric stretching vibration of CH_2, C=O stretching vibration, and symmetric stretching vibration of COO, respectively (Feng *et al.* 2017). The strong peak at around 1091 cm^{-1} was attributed to the overlapping of C-O-C stretching vibration and Si-O-Si asymmetric stretching vibration. This peak in the BC-RLs had a higher intensity, compared with that in the BCs, due to the higher content of the C-O-C group in the BC-RLs. These results demonstrated the successful binding of rhamnolipid onto the BCs.

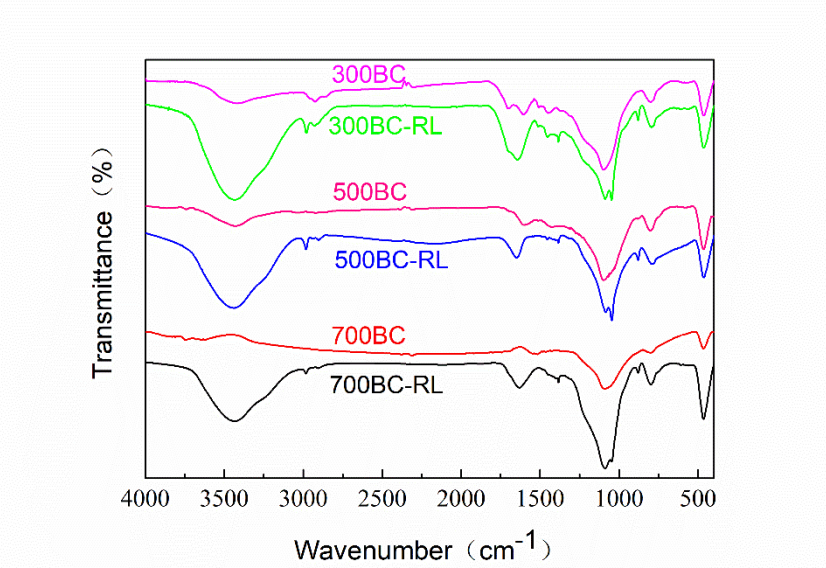

Fig. 3. FTIR spectra of the BCs and BC-RLs

To explore the chemical states of the different elements in the BC and BC-RL samples, the XPS spectra were recorded. Figure 4a shows that the wide-range scanning XPS spectra of the 700 BC and 700 BC-RL both exhibited peaks at around 103.2 eV, 284.5 eV, and 532.7 eV, which indicated the presence of Si, C, and O, respectively, in these materials. It was also noteworthy that all of the materials contained some Si, which may be explained by the presence of Si in the original rice husk. The C contents, O contents, and O/C ratios were calculated and are listed in Table 2. As was expected, the O/C ratio notably decreased as the pyrolysis temperature increased, which was caused by the loss of oxygen-containing groups during the pyrolysis process. The O/C ratio of the 300BC increased slightly after modification with rhamnolipid. In contrast, the O/C ratio increased noticeably when the 500 BC and 700 BC were modified with rhamnolipid, which indicated that the BC-RLs had higher oxygen contents than the original BCs. The high-resolution C 1s of the 700BC showed only one strong peak that was attributed to C-C/C=C, while the high-resolution C 1s of the 700BC-RL had three peaks that corresponded to C-C/C=C, C-O-C/C-O-H, and C=O. As is in accordance with the FTIR analysis, the XPS analysis further confirmed that more oxygen-containing functional groups were introduced to the modified materials.

Table 2. Element Content Calculated by the XPS Spectra

	300BC	300BC-RL	500BC	500BC-RL	700BC	700BC-RL
C (%)	43.48	43.87	53.56	50.27	75.21	70.86
O (%)	50.28	50.63	40.20	43.01	23.06	28.67
C/O ratio	1.15	1.15	0.75	0.86	0.31	0.41

The MB adsorption performances of the BCs and BC-RLs were compared. Figure 5 shows the MB removal efficiency increased from 41.8% to 64.5% when the pyrolysis temperature increased from 300 °C to 700 °C for the BCs. For the BC-RLs, the MB removal efficiency also increased with an increase in the pyrolysis temperature. Additionally, the BC-RLs showed remarkably higher removal efficiencies than the BCs prepared at the same temperatures, which demonstrated that modification with rhamnolipid improved the adsorption performance.

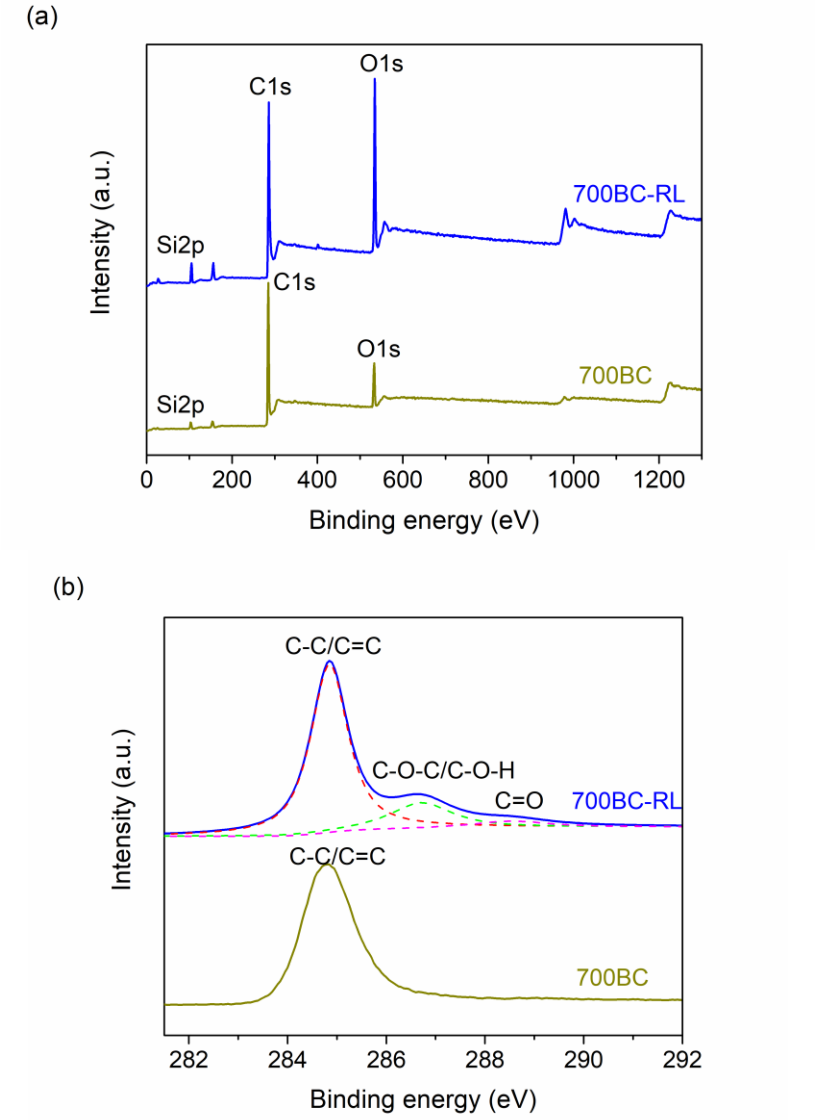

Fig. 4. Wide-range scanning XPS spectra (a) and high-resolution C 1s XPS spectra (b) of the 700BC and 700BC-RL

The adsorption of cationic dyes is highly dependent on the number of oxygen-containing functional groups on the carbonaceous materials, including carboxylic (-COOH) and hydroxyl (-OH) groups, because adsorption is mainly caused by the electrostatic attraction between cations and oxygen-containing functional groups (Ma *et al.* 2017). As a result of abundant oxygen-containing groups, the 700 BC-RL showed the highest MB removal efficiency (90.3%) among the test samples.

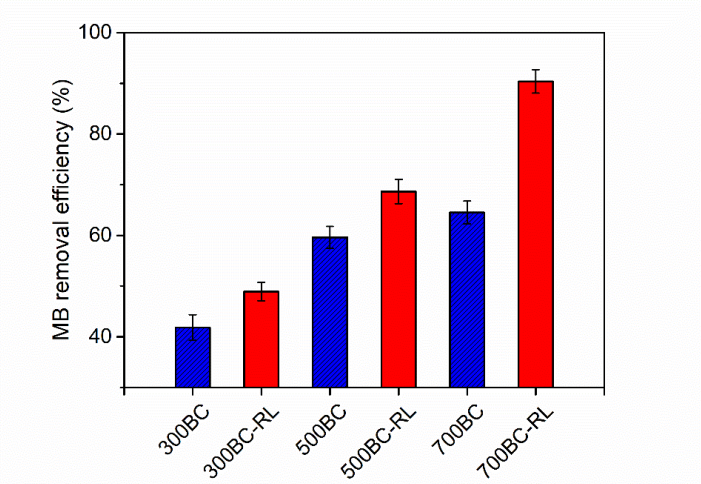

Fig. 5. MB removal efficiency of the BCs and BC-RLs; Experimental conditions: 50 mg of adsorbent added to 20 mL of MB solution (100 mg/L), pH = 7.0, equilibrium time = 72 h, temperature = 25 °C

In the subsequent experiment, the effect of the adsorbent loading on the MB adsorption was investigated, and the results are presented in Fig. 6. As was expected, the MB removal efficiency increased remarkably when the adsorbent loading increased from 10 mg/L to 50 mg/L. The MB removal efficiency increased slightly when the adsorbent loading was further increased from 50 mg/L to 70 mg/L. Additionally, it was apparent that the 700 BC-RL had a higher adsorption efficiency than the 300BC-RL and 500BC-RL because of its larger specific surface area and abundance of oxygen-containing functional groups.

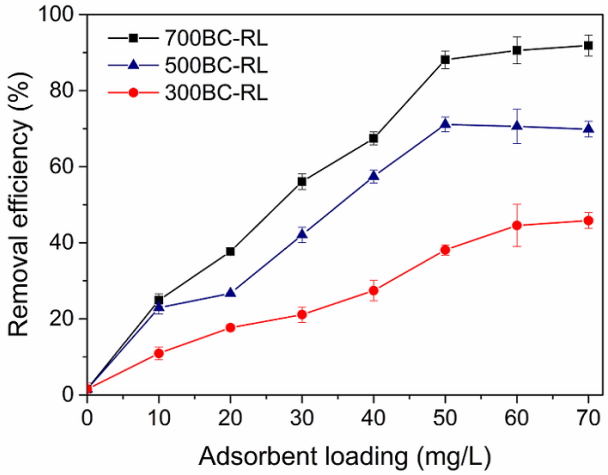

Fig. 6. Effect of the adsorbent loading on the removal efficiency; Experimental conditions: different amounts of adsorbent added to 20 mL of MB solution (100 mg/L), pH = 7.0, equilibrium time = 72 h, temperature = 25 °C

To study the mechanism of the adsorption process, the sorption kinetics of the MB onto the BCs and BC-RLs were analyzed using two commonly used kinetic models, which were the pseudo-first-order and pseudo-second-order models. The pseudo-first-order and pseudo-second-order models (Ho and McKay 1999) are shown below as Eqs. 3 and 4, respectively,

$$q_t = q_e\,(1 - \exp\,(-k_1\,t)) \tag{3}$$

$$q_t = \frac{k_2\,q_e^{\,2}\,t}{1 + k_2\,q_e\,t} \tag{4}$$

where q_e and q_t are the amount (mg/g) of MB adsorbed onto the adsorbent at equilibrium and a certain time t (h), respectively, k_1 is the rate constant of the pseudo-first-order model (h^{-1}), and k_2 is the rate constant of the pseudo-second-order model (g/mg·h).

The adsorption kinetics of MB adsorption onto the 700 BC and 700 BC-RL were shown in Fig. 7. The kinetic parameters and coefficients of determination (R^2) of the pseudo-first-order and pseudo-second-order models were calculated and summarized in Table 3. The correlation coefficient of the pseudo-second-order model for the 700BC and 700 BC-RL were 0.9895 and 0.9936, respectively, which were remarkably higher than those of the pseudo-first-order model (0.9323 and 0.9126, respectively). At the same time, the q_e value calculated from the pseudo-second-order model was consistent with the experimental adsorption capacity, while the q_e value calculated from the pseudo-first-order model obviously deviated from the experimental data. These results indicated that the pseudo-second-order kinetic model was more suitable for analyzing the adsorption data compared with the pseudo-first-order model. According to the pseudo-second-order model, the initial adsorption rates for the 700 BC and 700 BC-RL were 6.94 mg/g·h and 12.88 mg/g·h, respectively. Both the adsorption capacity and initial adsorption rates of the 700 BC-RL were obviously higher than those of the 700 BC, which demonstrated that modification with rhamnolipid could remarkably improve the adsorption rate.

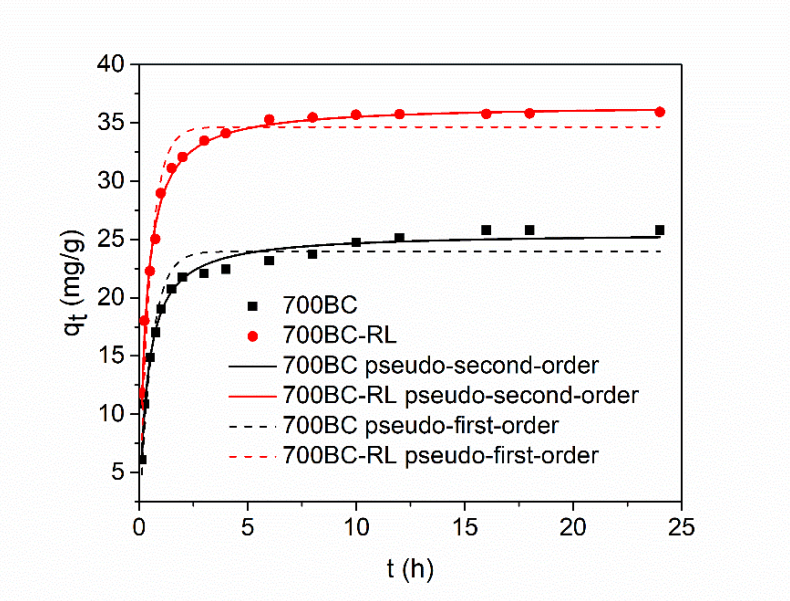

Fig. 7. Adsorption kinetics of MB adsorption onto the 700 BC and 700 BC-RL

Table 3. Kinetic Parameters for the Adsorption of MB by the 700 BC and 700 BC-RL

Adsorbent	Pseudo-first-order			Pseudo-second-order		
	k_1 (h^{-1})	q_e (mg/g)	R^2	k_2 (g/mg·h)	q_e (mg/g)	R^2
700 BC	1.808±0.18	23.97±0.47	0.9323	0.106±0.006	25.58±0.24	0.9895
700 BC-RL	2.042±0.21	34.66±0.69	0.9126	0.097±0.007	36.54±0.38	0.9936

When a solid adsorbent is used to remove dye from an aqueous solution through adsorption, the transfer of dye to the adsorbent is usually a multi-step process, and includes external mass transfer (film diffusion), intra-particle diffusion, or both (Wu *et al.* 2014). To elucidate the diffusion mechanism and rate controlling step, the intra-particle diffusion model was used to further analyze the data (Xu *et al.* 2012; Wang *et al.* 2016a). The intra-particle model is shown as Eq. 5,

$$q_t = k_d\, t^{1/2} + C \tag{5}$$

where k_d is the intra-particle diffusion rate constant (g/mg·$h^{1/2}$) and C is a constant (mg/g) corresponding to the contribution of the surface sorption to the rate controlling process.

Figure 8 shows the plot of q_t *versus* $t^{1/2}$ was composed of three stages, which suggested that the adsorption process involves multiple steps (Wang *et al.* 2016a). The first section of the plot with a large slope (Table 4) represented the film diffusion process, through which the MB was transported from the bulk solution to the external surface of the adsorbent. The second section of the plot corresponded to the intra-particle diffusion process, through which the MB molecules were transferred from the external surface to the inside of the adsorbent pores. The third section, which corresponded to the final equilibrium stage, had a slope approaching zero. This indicated that the intra-particle diffusion rate was very low at this stage (Wang *et al.* 2016a). The second sections of the plots for the 700 BC and 700 BC-RL did not pass through the origin point, which indicated that the intra-particle diffusion step took place in the adsorption process, but was not the only rate-limiting step (Wu *et al.* 2014).

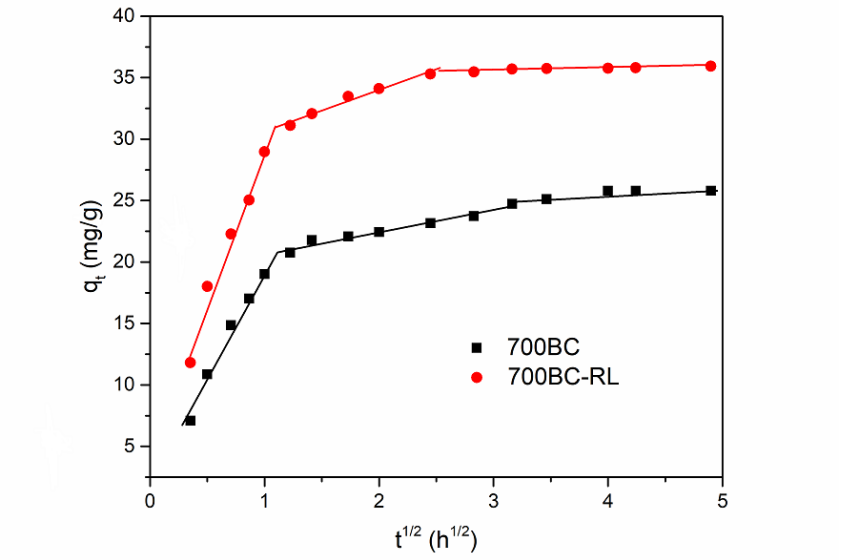

Fig. 8. Intra-particle diffusion plots for MB adsorption onto the 700 BC and 700 BC-RL

Table 4. Intra-particle Diffusion Parameters for MB Adsorption onto the 700 BC and 700 BC-RL

Adsorbent	700BC			700BC-RL		
	k_d (g/mg·h$^{1/2}$)	C (mg/g)	R^2	k_d (g/mg·h$^{1/2}$)	C (mg/g)	R^2
stage 1	19.36	0.30	0.9715	17.85	11.85	0.9377
stage 2	1.67	19.08	0.9553	0.89	30.26	0.9370
stage 3	0.65	22.89	0.7591	0.23	34.83	0.8617

To elucidate the interaction between the adsorbent and adsorbate at the adsorption equilibrium, three adsorption isotherm models, including the Langmuir, Freundlich, and BET models, were used to analyze the adsorption equilibrium data. The three isotherm models have been widely applied to describe the adsorption data of MB on carbon-based materials (Wu *et al.* 2014; Han *et al.* 2015; Fan *et al.* 2017). The Langmuir model is based on the hypothesis that adsorption takes place on a homogeneous surface through monolayer coverage, and the adsorbed species have no further interaction. The linear form of the Langmuir equation (Langmuir 1917) is shown as Eq. 6,

$$\frac{C_e}{q_e} = \frac{C_e}{q_m} + \frac{1}{q_m K_L} \quad (6)$$

where C_e represents the equilibrium concentration of MB in the solution (mg/L), q_e is the amount (mg/g) of adsorbate adsorbed onto the adsorbent at the equilibrium, q_m is the maximum adsorption capacity (mg/g) representing complete monolayer coverage (Xu *et al.* 2012), and K_L is the Langmuir constant (L/mg) that depends on the affinity of the binding sites and the adsorption energy.

The Freundlich model is an empirical model based on the assumption that the adsorption process occurs on heterogeneous surfaces though multilayer adsorption (Shen and Chen 2015). The linear form of the Freundlich model equation is expressed as Eq. 7,

$$\ln q_e = \frac{1}{\mathrm{n}} \ln C_e + \ln K_F \quad (7)$$

where K_F is the Freundlich constant corresponding to the adsorption capacity (L/mg), n is the constant related to the adsorption strength, and $1/n$ represents the adsorption favorability closely related to the degree of surface heterogeneity (Xu *et al.* 2012).

Based on the Langmuir model, the BET adsorption model assumes that multilayer adsorption occurs on the adsorbent surface (Wu *et al.* 2014). It also assumes that the adsorption of the first monolayer and each successive layer depends on the adsorption energy and condensation energy, respectively (Nekouei and Nekouei 2017). The linear form of the BET equation (Brunauer *et al.* 1938) is expressed as Eq. 8,

$$\frac{C_e}{(C_e - C_s) q_e} = \frac{(K_b - 1) C_e}{K_b q_{max} C_s} + \frac{1}{K_b q_{max}} \quad (8)$$

where C_s represents the saturation concentration of the solute (mg/L), q_e corresponds to the final amount of adsorbate adsorbed onto the adsorbent (mg/g), q_{max} is the amount of solute adsorbed to form a complete monolayer (mg/g) (Nekouei and Nekouei 2017), and K_b is the BET constant.

The adsorption isotherms of the MB onto the 700 BC-RL at 25 °C, 35 °C, and 45 °C are exhibited in Fig. 9.

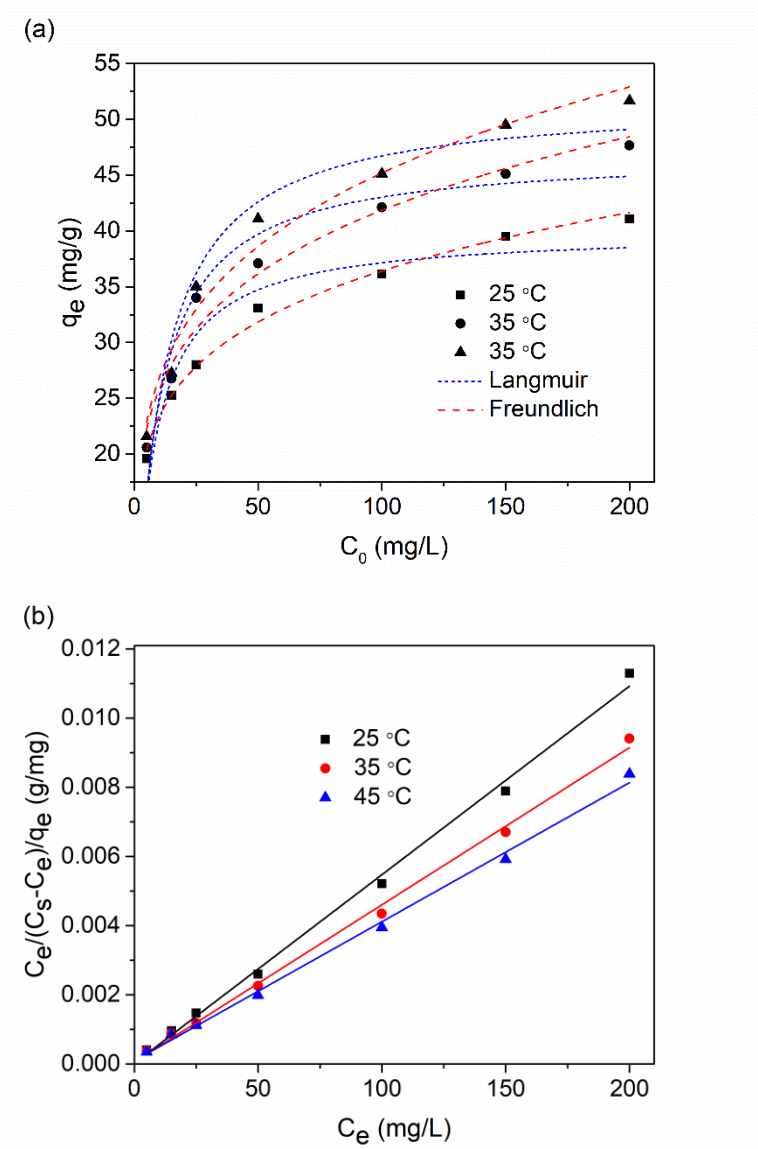

Fig. 9. Adsorption isotherms fitted by the Langmuir (a), Freundlich (a), and BET (b) models

It was observed that the amount of MB adsorbed onto the 700 BC-RL increased with an increase in the MB equilibrium concentration and reached saturation gradually for all of the tested temperatures. When the temperature increased from 25 °C to 45 °C, the amount of MB adsorbed onto the 700 BC-RL obviously increased, which was consistent with previous reports (Wu *et al.* 2014; Fan *et al.* 2017). The regression parameters of the Langmuir, Freundlich, and BET models were calculated and listed in Table 5. The coefficients of determination for the different models increased in the following order: Langmuir < Freundlich < BET. This suggested that the BET model fitted the isotherms better than the Freundlich and Langmuir models. The coefficients of determination of the BET model all exceeded 0.995 at the three tested temperatures, which indicated that the BET model ideally fitted the isotherms of MB adsorption onto the BC-RL. This result also supported the conclusion that the adsorption of MB onto the surface of the 700 BC-RL involved multilayer formation. Previous studies reported that the isotherms of MB adsorption onto BC (Fan *et al.* 2017), graphene oxide, and graphene (Shen and Chen 2015)

were better fitted by the Langmuir model than the Freundlich model, which suggested that the adsorption of MB onto these carbon-based materials tends toward monolayer adsorption rather than multilayer adsorption. In contrast, it has also been reported that the BET model fitted the isotherms better than the Langmuir and Freundlich model for surfactant-modified graphene oxides (Wu *et al*. 2014), which is consistent with the phenomenon observed in this study. These results indicated that modification of carbon-based materials with surfactant could alter the adsorption process from monolayer adsorption to multilayer adsorption process. This is probably due to the electrostatic interaction between the MB and the oxygen-containing groups from surfactant (Wu *et al*. 2014).

Table 5. Isotherm Parameters for the Adsorption of MB by the 700BC-RL

Isotherm	Parameter	Temperature (°C)		
		25	35	45
Langmuir	K_L (L/mg)	0.1329±0.0316	0.1099±0.0228	0.0932±0.0198
	q_m (mg/g)	39.95±1.76	46.94±1.93	51.73±2.31
	R^2	0.9064	0.9353	0.9361
Freundlich	K_F (L/mg)	14.94±0.53	15.84±1.15	15.87±1.24
	1/*n*	5.17±0.21	4.74±0.36	4.40±0.34
	R^2	0.9929	0.9762	0.9767
BET	K_b	1929.66±32.75	512.51±12.09	287.14±8.21
	q_{max} (mg/g)	29.05±0.95	33.99±1.02	37.49±1.27
	R^2	0.9965	0.9971	0.9968

In order to elucidate the influence of temperature on the adsorption of MB onto 700BC-RL, the thermodynamic parameters, including Gibbs free energy (ΔG^0), enthalpy (ΔH^0) and entropy (ΔS^0) were calculated according to the following equations,

$$\Delta G^0 = -RT \ln K_L \quad (9)$$

$$\Delta G^0 = \Delta H^0 - T\Delta S^0 \quad (10)$$

where K_L is Langmuir constant when concentration terms are expressed in milligrams per gram, R (8.314 J/mol K) is the universal gas constant and T (K) is the absolute temperature. The ΔH^0 and ΔS^0 values were calculated from the slope and intercept of the plot of ΔG^0 versus T. As shown in Table 6, ΔG^0 values were negative, indicating the spontaneity of the adsorption processes. The lower ΔG^0 value at higher temperature suggests that adsorption of MB onto 700BC-RL becomes more favorable with increasing temperature. The ΔH^0 value is positive, indicating that the adsorption processes are endothermic in nature. The positive value of ΔS^0 confirms the increase of randomness at solid-solution interface.

Table 6. Thermodynamic parameters for MB adsorption onto the 700BC-RL

Temperature (°C)	ΔG^0 (kJ/mol)	ΔS^0 (J/K·mol)	ΔH^0 (kJ/mol)
25 (298 K)	-29.23	51.2	13.97
35 (308 K)	-29.72		
45 (318 K)	-30.25		

To confirm the adsorption of MB, the FT-IR spectra (Fig. 10) of initial 700BC-RL, MB and the 700BC-RL with adsorbed MB were investigated. For the FT-IR spectra of MB, the peaks at 1592 and 1385 cm^{-1} were attributed to the stretching vibrations of C=N (and C=C) and C-N bonds in the heterocycle of MB, respectively. The peaks at 1353 and 1324 cm^{-1} were attributed to the stretching vibration of C-N bond connected with benzene ring and N-CH_3 bond, respectively. The peaks at about 1488 and 1387 cm^{-1} were attributed to the CH_2 and CH_3 deformation vibration, respectively. The peaks at about 1246 and 1212 cm^{-1} were due to Ar-N deformation vibration. The peaks at around 1169 and 1133 cm^{-1} were attributed to the stretching vibrations of C=S and C-S, respectively, and the peak at about 882 cm^{-1} was attributed to the wagging vibration of C-H aromatic ring of MB. The FTIR spectra of the 700BC-RL with adsorbed MB exhibited the characteristic peaks at 1347 and 1321 cm^{-1}, corresponding to the stretching vibration of C-N bond connected with benzene ring and N-CH_3 bond, respectively. Moreover, the intensity of the peak of 1385 cm^{-1} increased owing to the overlap of the symmetric stretching vibration of COO and stretching vibrations of C-N bonds from MB. These results confirmed the presence of MB on the surface of adsorbent.

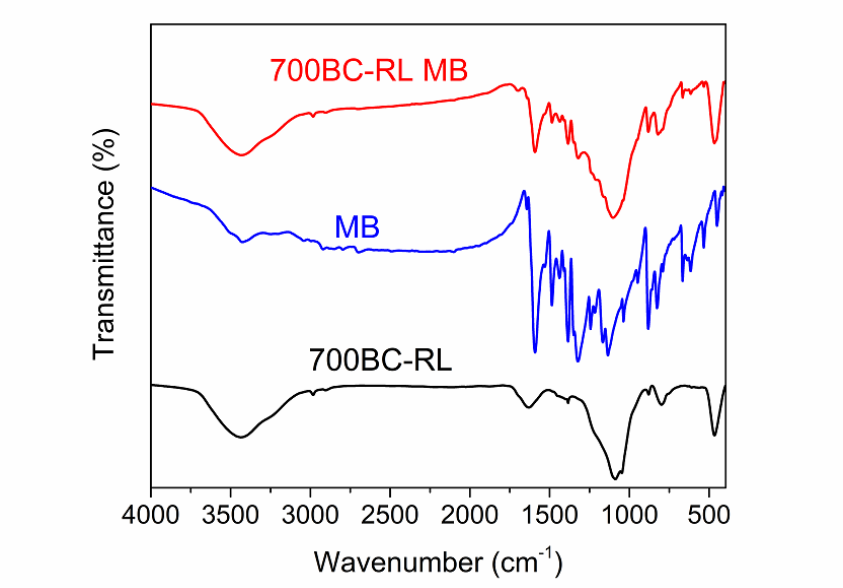

Fig. 10. FT-IR spectra of 700BC-RL, MB and 700BC-RLwith adsorbed MB

For the desorption study, 50 mg of adsorbent was added to 20 mL of MB solution with initial MB concentration of 100 mg/L (pH=6.0) at 25 °C. After adsorption, the used adsorbent was added into deionized water, 0.3 M NaOH or 0.3 M HCl solution, and stirred for 2 h. As shown in Fig. 11a, 0.3 M NaOH solution was very effective for desorption of MB from 700 BC-RL. More than 90% of MB was desorbed from 700 BC-RL by 0.3 M NaOH solution within 2 h. After washing with 0.3 M NaOH or 0.3 M HCl solution under stirring for 2 h to remove MB, the 700 BC-RL were washed with deionized water five times to remove the residual NaOH or HCl. The 700 BC-RL was regenerated through vacuum freeze drying and reused for adsorption. When 0.3M NaOH solution was used to regenerate 700 BC-RL, the MB removal rate still reached 82.7% after three cycles of recycling (Fig. 11b). In contrast, the MB removal rate decreased remarkably when the 700 BC-RL was regenerated by 0.3 M HCl solution.

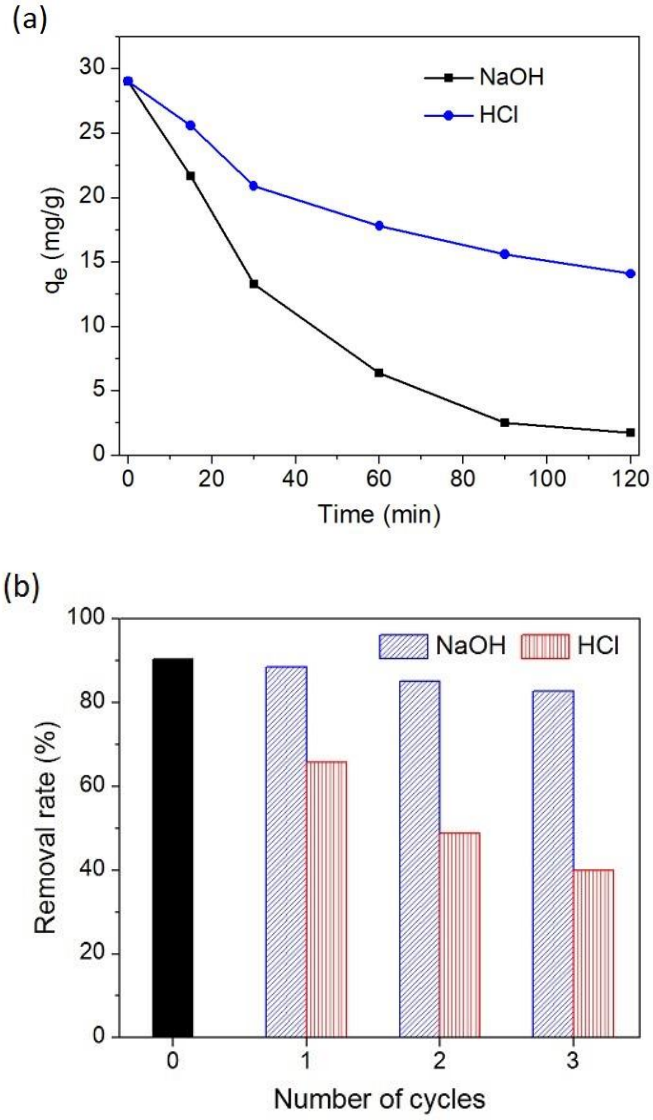

Fig. 11. (a) Desorption of MB from 700 BC-RL and (b) MB removal rate of the reused 700 BC-RL

The MB adsorption capacity of 700 BC-RL developed in the present work is higher than original biomass (Suhas *et al.* 2016) and biochar without post-modification (Fan *et al.* 2017). Although the MB adsorption capacity of 700 BC-RL is lower than commercially available activated charcoal (Liu *et al.* 2015), biochar activated by KOH, graphene based material (Wu *et al.* 2014) is cheap and environmentally friendly owing to the convenient preparation process. Therefore, these results suggested that BC-RL is a promising adsorbent for the removal of organic pollutants from aqueous solutions.

CONCLUSIONS

1. The BC-RLs were prepared though a one-step method and were used to investigate the adsorptive removal of MB from an aqueous solution.

2. The characterizations suggested that the BC-RLs had more abundant functional groups and a lower specific surface area compared with the unmodified BCs.
3. The BC-RLs showed remarkably higher MB removal efficiencies than the unmodified BCs, which demonstrated that modification with rhamnolipid could remarkably improve the adsorption performance of BCs.
4. The pseudo-second-order kinetic model was more suitable than the pseudo-first-order model and fit the adsorption kinetic data.
5. Among the three isotherm models, the BET model fit the isotherms of MB adsorption onto the BC-RL the best. This indicated that the adsorption of MB onto the surface of the 700 BC-RL involved a multilayer formation process.
6. This work suggested BC-RL is an environmentally benign and cost-effective adsorbent that can remove organic pollutants from aqueous solutions.

ACKNOWLEDGMENTS

The authors are grateful for the support of the National Water Pollution Control and Treatment Science and Technology Major Project (Grant No. 2015ZX07203-011-06), Engineering Research Center Program of Tianjin (17PTGCCX00240). This work was also supported by the National Natural Science Foundation of China (Grant No. 41473070).

REFERENCES CITED

Ashworth, A. J., Sadaka, S. S., Allen, F. L., Sharara, M. A., and Keyser, P. D. (2014). "Influence of pyrolysis temperature and production conditions on switchgrass biochar for use as a soil amendment," *BioResources* 9(4), 7622-7635. DOI: 10.15376/biores.9.4.7622-7635

Beesley, L., Moreno-Jiménez, E., Gomez-Eyles, J. L., Harris, E., Robinson, B., and Sizmur, T. (2011). "A review of biochars' potential role in the remediation, revegetation and restoration of contaminated soils," *Environ. Pollut.* 159(12), 3269-3282. DOI: 10.1016/j.envpol.2011.07.023

Brunauer, S., Emmett, P. H., and Teller, E. (1938). "Adsorption of gases in multimolecular layers," *J. Am. Chem. Soc.* 60(2), 309-319. DOI: 10.1021/ja01269a023

Chen, H., Wang, X., Li, J., and Wang, X. (2015). "Cotton derived carbonaceous aerogels for the efficient removal of organic pollutants and heavy metal ions," *J. Mater. Chem. A* 3(11), 6073-6081. DOI: 10.1039/C5TA00299K

Chen, X., Chen, Q., Jiang, W., Wei, Z., and Zhu, Y. (2017). "Separation-free TiO_2-graphene hydrogel with 3D network structure for efficient photoelectrocatalytic mineralization," *Appl. Catal. B-Environ.* 211, 106-113. DOI: 10.1016/j.apcatb.2017.03.061

Cui, L., Chen, T., Quan, G., Xiao, B., Ma, Y., Pan, M., Liu, Y., Liu, B., Yin, C., Yan, J., *et al.* (2017). "Renewable material-derived biochars for the efficient removal of 2,4-dichlorophen from aqueous solution: Adsorption/desorption mechanisms," *BioResources* 12(3), 4912-4925. DOI: 10.15376/biores.12.3.4912-4925

Deng, H., Yu, H., Chen, M., and Ge, C. (2014). "Sorption of atrazine in tropical soil by biochar prepared from cassava waste," *BioResources* 9(4), 6627-6643. DOI: 10.15376/biores.9.4.6627-6643

Ding, Z., Wu, H., and Hu, X. (2017). "Multiple characterization for mechanistic insights of Pb(II) sorption onto biochars derived from herbaceous plant, biosolid, and livestock waste," *BioResources* 12(3), 6763-6772. DOI: 10.15376/biores.12.3.6763-6772

Ersan, G., Apul, O. G., Perreault, F., and Karanfil, T. (2017). "Adsorption of organic contaminants by graphene nanosheets: A review," *Water Res.* 126, 385-398. DOI: 10.1016/j.watres.2017.08.010

Fan, S., Wang, Y., Wang, Z., Tang, J., Tang, J., and Li, X. (2017). "Removal of methylene blue from aqueous solution by sewage sludge-derived biochar: Adsorption kinetics, equilibrium, thermodynamics and mechanism," *Journal of Environmental Chemical Engineering* 5(1), 601-611. DOI: 10.1016/j.jece.2016.12.019

Feng, D., Zhao, Y., Zhang, Y., Zhang, Z., Zhang, L., Gao, J., and Sun, S. (2017). "Synergetic effects of biochar structure and AAEM species on reactivity of H_2O-activated biochar from cyclone air gasification," *Int. J. Hydrogen Energ.* 42(25), 16045-16053. DOI: 10.1016/j.ijhydene.2017.05.153

Gaber, D., Haija, M. A., Eskhan, A., and Banat, F. (2017). "Graphene as an efficient and reusable adsorbent compared to activated carbons for the removal of phenol from aqueous solutions," *Water Air Soil Poll.* 228(9), 320-333. DOI: 10.1007/s11270-017-3499-x

Han, X., Chu, L., Liu, S., Chen, T., Ding, C., Yan, J., Cui, L., and Quan, G. (2015). "Removal of methylene blue from aqueous solution using porous biochar obtained by KOH activation of peanut shell biochar," *BioResources* 10(2), 2836-2849. DOI: 10.15376/biores.10.2.2836-2849

Ho, Y. S., and McKay, G. (1999). "Pseudo-second order model for sorption processes," *Process Biochem.* 34(5), 451-465. DOI: 10.1016/S0032-9592(98)00112-5

Hou, Q., Ju, M., Li, W., Liu, L., Chen, Y., and Yang, Q. (2017). "Pretreatment of lignocellulosic biomass with ionic liquids and ionic liquid-based solvent systems," *Molecules* 22(3), 490, 1-24. DOI: 10.3390/molecules22030490

Hou, Q., Li, W., Ju, M., Liu, L., Chen, Y., and Yang, Q. (2016). "One-pot synthesis of sulfonated graphene oxide for efficient conversion of fructose into HMF," *RSC Adv.* 6(106), 104016-104024. DOI: 10.1039/C6RA23420H

Hou, Q., Li, W., Ju, M., Liu, L., Chen, Y., Yang, Q., and Wang, J. (2015). "Separation of polysaccharides from rice husk and wheat bran using solvent system consisting of BMIMOAc and DMI," *Carbohyd. Polym.* 133, 517-523. DOI: 10.1016/j.carbpol.2015.07.059

Hou, Q., Zhen, M., Liu, L., Chen, Y., Huang, F., Zhang, S., Li, W., and Ju, M. (2018). "Tin phosphate as a heterogeneous catalyst for efficient dehydration of glucose into 5-hydroxymethylfurfural in ionic liquid," *Appl. Catal. B-Environ.* 224, 183-193. DOI: 10.1016/j.apcatb.2017.09.049

Hu, X., and Zhou, Q. (2013). "Health and ecosystem risks of graphene," *Chem. Rev.* 113(5), 3815-3835. DOI: 10.1021/cr300045n

Inyang, M., and Dickenson, E. (2015). "The potential role of biochar in the removal of organic and microbial contaminants from potable and reuse water: A review," *Chemosphere* 134, 232-240. DOI: 10.1016/j.chemosphere.2015.03.072

Kermanioryani, M., Mutalib, M. I. A., Kurnia, K. A., Lethesh, K. C., Krishnan, S., and Leveque, J.-M. (2016). "Enhancement of π–π aromatic interactions between hydrophobic ionic liquids and methylene blue for an optimum removal efficiency and assessment of toxicity by microbiological method," *J. Clean. Prod.* 137, 1149-1157. DOI: 10.1016/j.jclepro.2016.07.193

Kumar, V., Kim, K.-H., Park, J.-W., Hong, J., and Kumar, S. (2017). "Graphene and its nanocomposites as a platform for environmental applications," *Chem. Eng. J.* 315, 210-232. DOI: 10.1016/j.cej.2017.01.008

Langmuir, I. (1917). "The constitution and fundamental properties of solids and liquids. II. Liquids," *J. Am. Chem. Soc.* 39(9), 1848-1906. DOI: 10.1021/ja02254a006

Liu, B., Li, Y., Gai, X., Yang, R., Mao, J., and Shan, S. (2016). "Exceptional adsorption of phenol and *p*-nitrophenol from water on carbon materials prepared *via* hydrothermal carbonization of corncob residues," *BioResources* 11(3), 7566-7579. DOI: 10.15376/biores.11.3.7566-7579

Liu, W.-J., Jiang, H., and Yu, H.-Q. (2015). "Development of biochar-based functional materials: Toward a sustainable platform carbon material," *Chem. Rev.* 115(22), 12251-12285. DOI: 10.1021/acs.chemrev.5b00195

Ma, Q., Yu, Y., Sindoro, M., Fane, A. G., Wang, R., and Zhang, H. (2017). "Carbon-based functional materials derived from waste for water remediation and energy storage," *Adv. Mater.* 29(13), 1605361. DOI: 10.1002/adma.201605361

Mohan, D., Sarswat, A., Ok, Y. S., and Pittman, C. U. (2014). "Organic and inorganic contaminants removal from water with biochar, a renewable, low cost and sustainable adsorbent – A critical review," *Bioresource Technol.* 160, 191-202. DOI: 10.1016/j.biortech.2014.01.120

Negueroles, P. G., Bou-Belda, E., Santos-Juanes, L., Amat, A. M., Arques, A., Vercher, R. F., Monllor, P., and Vicente, R. (2017). "Treatment and reuse of textile wastewaters by mild solar photo-Fenton in the presence of humic-like substances," *Environ. Sci. Pollut. R.* 24(14), 12664-12672. DOI: 10.1007/s11356-016-7889-1

Nekouei, F., and Nekouei, S. (2017). "Comments on the paper "Adsorptive removal of methylene blue by rhamnolipid-functionalized graphene oxide from wastewater"," *Water Res.* 108, 462-463. DOI: 10.1016/j.watres.2016.10.061

Ribeiro, R. S., Rodrigues, R. O., Silva, A. M. T., Tavares, P. B., Carvalho, A. M. C., Figueiredo, J. L., Faria, J. L., and Gomes, H. T. (2017). "Hybrid magnetic graphitic nanocomposites towards catalytic wet peroxide oxidation of the liquid effluent from a mechanical biological treatment plant for municipal solid waste," *Appl. Catal. B-Environ.* 219, 645-657. DOI: 10.1016/j.apcatb.2017.08.013

Shen, Y., and Chen, B. (2015). "Sulfonated graphene nanosheets as a superb adsorbent for various environmental pollutants in water," *Envir. Sci. Tech.* 49(12), 7364-7372. DOI: 10.1021/acs.est.5b01057

Singh, B., Singh, B. P., and Cowie, A. L. (2010). "Characterisation and evaluation of biochars for their application as a soil amendment," *Aust. J. Soil Res.* 48(7), 516-525. DOI: 10.1071/SR10058

Suhas, Gupta, V. K., Carrott, P. J. M., Singh, R., Chaudhary, M., and Kushwaha, S. (2016). "Cellulose: A review as natural, modified and activated carbon adsorbent," *Bioresource Technol.* 216, 1066-1076. DOI: 10.1016/j.biortech.2016.05.106

Tan, X., Liu, Y., Zeng, G., Wang, X., Hu, X., Gu, Y., and Yang, Z. (2015). "Application of biochar for the removal of pollutants from aqueous solutions," *Chemosphere* 125, 70-85. DOI: 10.1016/j.chemosphere.2014.12.058

Wang, J., Chen, B., and Xing, B. (2016a). "Wrinkles and folds of activated graphene nanosheets as fast and efficient adsorptive sites for hydrophobic organic contaminants," *Envir. Sci. Tech.* 50(7), 3798-3808. DOI: 10.1021/acs.est.5b04865

Wang, P., Zhou, X., Zhang, Y., Wang, L., Zhi, K., and Jiang, Y. (2016b). "Synthesis and application of magnetic reduced graphene oxide composites for the removal of bisphenol A in aqueous solution - A mechanistic study," *RSC Adv.* 6(104), 102348-102358. DOI: 10.1039/C6RA23542E

Wu, Y., Luo, H., Wang, H., Wang, C., Zhang, J., and Zhang, Z. (2013). "Adsorption of hexavalent chromium from aqueous solutions by graphene modified with cetyltrimethylammonium bromide," *J. Colloid Interf. Sci.* 394, 183-191. DOI: 10.1016/j.jcis.2012.11.049

Wu, Z., Zhong, H., Yuan, X., Wang, H., Wang, L., Chen, X., Zeng, G., and Wu, Y. (2014). "Adsorptive removal of methylene blue by rhamnolipid-functionalized graphene oxide from wastewater," *Water Res.* 67, 330-344. DOI: 10.1016/j.watres.2014.09.026

Xi, X., Yan, J., Quan, G., and Cui, L. (2014). "Removal of the pesticide pymetrozine from aqueous solution by biochar produced from Brewer's spent grain at different pyrolytic temperatures," *BioResources* 9(4), 7696-7709. DOI: 10.15376/biores.9.4.7696-7709

Xu, J., Wang, L., and Zhu, Y. (2012). "Decontamination of bisphenol A from aqueous solution by graphene adsorption," *Langmuir* 28(22), 8418-8425. DOI: 10.1021/la301476p

Zhang, J., Liu, J., and Liu, R. (2015). "Effects of pyrolysis temperature and heating time on biochar obtained from the pyrolysis of straw and lignosulfonate," *Bioresource Technol.* 176, 288-291. DOI: 10.1016/j.biortech.2014.11.011

Zheng, R., Chen, Z., Cai, C., Wang, X., Huang, Y., Xiao, B., and Sun, G. (2013). "Effect of biochars from rice husk, bran, and straw on heavy metal uptake by pot-grown wheat seedling in a historically contaminated soil," *BioResources* 8(4), 5965-5982. DOI: 10.15376/biores.8.4.5965-5982

Article submitted: December 5, 2017; Peer review completed: February 16, 2018; Revised version received and accepted: February 28, 2018; Published: March 6, 2018.
DOI: 10.15376/biores.13.2.3061-3081

APPENDIX

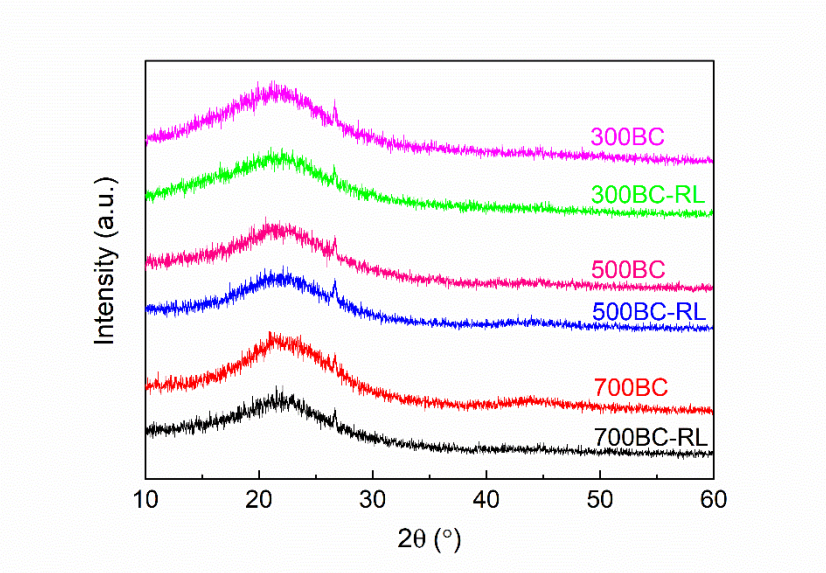

Complimentary Fig. 1. XRD spectra of the BCs and BC-RLs

The XRD patterns (Complimentary Fig. 1) all showed a broad dominant peak at around 22.4°, which was attributed to the typical structure of biochar-based materials (Singh *et al.* 2010). Additionally, all of the materials showed a very small sharp peak at around 26.6°, which corresponded to SiO_2 (Zheng *et al.* 2013; Hou *et al.* 2015). This was in accordance with the subsequent FTIR and XPS analyses. The XRD analysis indicated that the crystal structure of BC is not changed after modification with rhamnolipid.